Korean J. Chem. Eng., 34(2), 328-339 (2017)
DOI: 10.1007/s11814-016-0295-z

pISSN: 0256-1115
eISSN: 1975-7220

Hybrid nanocomposite membranes of sulfonated poly(ethersulfone)/1,1-carbonyl diimidazole/1-(3-aminopropyl)-silane/silica for direct methanol fuel cells

Yasamin Khosravi*, Shadi Hassanajili,†, Mohammad Hosein Moslemin*, and Masumeh Tabatabaei***

*Department of Chemistry, Yazd Branch, Islamic Azad University, Yazd, Iran
**School of Chemical and Petroleum Engineering, Shiraz University, 71348-51154 Shiraz, Iran
(*Received 12 February 2016 • accepted 17 October 2016*)

Abstract−Composite membranes of sulfonated poly(ethersulfone)/1,1-carbonyl diimidazole/1-(3-aminopropyl)-silane/silica (SPES/CDI/AS/SiO_2) with silica of various contents (3, 5 and 8 wt%) were prepared as electrolytes for direct methanol fuel cells (DMFCs). Comparison was made with pure SPES and SPES/SiO_2. The properties of the composite membranes were studied by FTIR, TGA, XRD, water and methanol uptake, proton conductivity. SPES/CDI/AS/SiO_2 membranes were also characterized by scanning electron microscopy (SEM), which showed good adhesion between the modified sulfonic acid (-SO_3H) groups of SPES and silica because of cross-linking with covalent bond formation and reduced cavities in the composites. This effect played an important role in reducing water uptake, methanol uptake and methanol permeability of the SPES/CDI/AS/SiO_2 composites. The water and methanol uptake and also methanol permeability of the SPES/CDI/AS/SiO_2 composite membrane with 8% SiO_2 were found in the order 3.58%, 2.48% and 1.91×10^{-7} (cm^2s^{-1}), lower than those of SPES and Nafion 117. In SPES membrane of 16.94% level of sulfonation, the proton conductivity was 0.0135 s/cm at 25 °C, which approached that of Nafion 117 under the same conditions. Also, the proton conductivity of the SPES/CDI/AS/SiO_2 8% membrane was 0.0186 s/cm, which was higher than that of SPES at room temperature. The preparation of SPES/SiO_2 composites in the presence of AS and CDI, led to 63%, 56% and 64% reduction of water uptake, methanol uptake and methanol permeability, respectively without a sharp drop in proton conductivity of the composite membranes which featured a good balance between high proton conductivity, water and methanol uptake of SPES/CDI/AS/SiO_2 membranes.

Keywords: Membrane, Sulfonated Poly(ethersulfone), Silica, Nafion 117, Methanol Permeability, Proton Conductivity

INTRODUCTION

In recent years, with the shortage of conventional energy resources, there has been a great advancement in the study of fuel cells as important energy alternatives. Such systems are promising candidates for energy generation due to their superior energy density, with convenient storage and transport and low pollution emissions in the environment. Hydrogen-methanol fuel cells are good choices for producing energy in portable devices such as laptops, cell phone, and means of transportation. Simplicity and small size of these cells and low operation temperature are the reasons for their extensive application in portable devices [1-5]. One of the main components in such fuel cells is an electrolyte membrane whose main function is to carry protons and capture and trap methanol. The first polymeric membrane used in methanol fuel cells was Nafion, a sulfonated tetrafluoroethylene based fluoropolymer-copolymer, synthesized by Walther Grot of DuPont [6]. Nafion has been suitable for fuel cells due to its high proton conductivity and thermal stability, though it is highly permeable to methanol crossover, which not only wastes the fuel but reduces membrane application in fuel cells containing methanol [7]. Therefore, fuel cells containing methanol could be optimized through optimization membranes [8-10]. Recently, various research reports have recommended several kinds of aromatic hydrocarbons to replace Nafion in fuel cell membrane application [11-17]. Among these aromatic hydrocarbons, polyether ether ketone (PEEK) and polyether sulfone (PES) are being used as electrolytes in fuel cells containing methanol. They are both cheap and easy to synthesize and produce. They have also high chemical and mechanical resistance and excellent thermal stability [18-24]. To increase conductivity in such polymers, ionomeric groups like sulfonic acid groups are attached to aromatic polymers through sulfonation method [25,26]. Therefore, proton conductivity in polymeric membrane increases, while it is directly related to the degree of sulfonation. In the present work, poly(ethersulfone) was selected for its superior properties as a polymer electrolyte membrane functionalized by insertion of sulfonic acid groups in the polymeric backbone. It is reported that the conductivity in polymers with aromatic structure (e.g., PES) is increased with sulfonation degree and has a strong impact on conductivity and membrane stability [27-29].

Wilhelm [30] discovered that when sulfonation degree is below 0.4, polymer dissolves in standard solvents that are used for membrane formation [31]. Sulfonated aromatic polymers are expected to exhibit much higher ion exchange capacity (IEC) in comparison to fluorinated membrane to reach the same conductivity [32-34]. Unfortunately, higher IEC leads to morphological instability and large swelling in the membrane [32-34]. One solution in solving this

†To whom correspondence should be addressed.
E-mail: ajili@shirazu.ac.ir

problem is to add minerals to polymer membrane for improving polymers' physiochemical properties, such as elasticity, proton conductivity, methanol and water crossover, hydrophilic properties and thermal stability [35-37].

As mentioned, Nafion has been the standard membrane for DMFCs; while, it is highly permeable toward methanol through the water filled pores of the membrane, resulting in the oxidation of cathode, fuel consumption and energy efficiency loss [38-40]. Therefore, a new approach can be made to develop proton conducting membrane with high selectivity and low methanol permeability as complete replacement of Nafion for DMFCs. Our main purpose was to develop an alternative membrane based on SPES nanocomposites to provide an effective method to reduce water and methanol crossover in SPES membranes by in situ synthesis of inorganic SiO_2 in the presence of 1,1-carbonyl diimidazole (CDI) and 1-(3-aminopropyl)-silane (AS). SPES/CDI/AS/SiO_2 composite membranes with various percentages of 3, 5 and 8 wt% SiO_2 were produced in laboratory. These composite membranes were studied for their morphological properties, methanol and water uptake, thermal stability, XRD and conductivity. Through this study, we found that adding CDI and AS to the polymeric matrix results in better and more uniform distribution of SiO_2 particles in polymeric matrix and excitingly low methanol permeability and high membrane selectivity compared to Nafion 117.

EXPERIMENTAL

1. Materials

PES polymer (E6020P, M_w 51,000 g/mol) was provided by BASF Co. The sulfonic acid (95-98%), the inorganic precursor tetraethoxysilane (TEOS), and 1,1′-carbonyl-diimidazole (CDI) were received from the Merck. The solvent, *N,N*-methyl formamide (DMF) was purchased from the Applichem GmbH Co. and 1-(3-aminopropyl)-silane (AS) was supplied by Aldrich.

2. Sulfonation of Poly(ethersulfone)

PES polymer (E6020P, M_w 51,000 g/mol) was sulfonated as described below. This polymer was dried in a vacuum oven for 24 h at 60 °C. A 4 g of polymer was dissolved in 70 ml of concentrated sulfuric acid (95-98%) and the solution was kept stirred for 24 h at 55 °C. In the next step, the polymer solution was poured in excess of ice-cold water under continuous stirring, obtaining a white precipitate. After standing overnight, the precipitate was filtered and washed several times to neutral pH. The sulfonated polymer was dried in a vacuum oven for 24 h at the temperature of 60-80 °C (Fig. 1).

3. Preparation of SPES Membranes

Membranes were prepared by dissolving 1.0 g of SPES in *N,N*-dimethyl formamide (DMF) to give a 10 wt% solution. After dissolution, the resulting SPES mixture solutions were filtered. Subsequently, the polymer solution was cast onto a flat glass plate to give a thin film. The cast membrane was allowed to evaporate the DMF solvent and dried in a vacuum oven at 60 °C for 48 h, followed by 120 °C for 24 h. After evaporation of the solvent and cooling to room temperature, the resultant membrane was peeled off from the glass in de-ionized water.

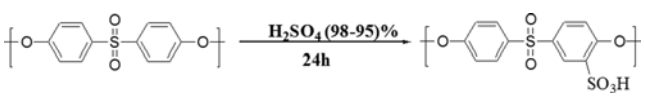

Fig. 1. Schematic presentation of the reaction between sulfuric acid and PES.

4. Preparation of SPES/SiO_2 Composite Membrane

The SPES polymer was dissolved in DMF to produce a 10 wt% solution. A composite membrane, based on SPES and TEOS, was prepared by adding TEOS to DMF. After 30 min of stirring, milliQ-water was added for partial hydrolyzation of TEOS (n_{H_2O}/n_{TEOS}=2/1).Polymer solution was added after stirring the mixture for 3 h and stirring was continued for two days at room temperature. It was then poured on a glass plate and heated in a vacuum oven for 30 h at 60 °C for solvent removal.

5. Preparation of SPES/CDI/AS/SiO_2

First, the SPES polymer was dissolved in DMF to make a 10 wt% solution. In the second stage, 0.2 g CDI was added into polymer solution and stirred for 2 days at 55 °C. In the third stage, 0.12 g AS and 0.1 g water were added into the mixture and continued stirring for 2 days. Finally, TEOS was added into the polymer solution and stirred for two days at room temperature. SiO_2 nanoparticles were produced in-situ by sol-gel reaction of TEOS in SPES matrix. The thickness of the produced composite membranes was between 50-100 mm.

CHARACTERIZATION METHODS

1. Proton Nuclear Magnetic Resonance Spectroscopy (NMR)

The ^{1}H NMR spectra were recorded on a Bruker Advance NMR spectrometer at a resonance frequency of 250 MHz. Polymer solutions of 2 wt% were prepared in dimethylsulfoxide-d6 (DMSO-d6) and tetramethylsilane (TMS) was used as an internal standard.

2. Fourier Transform Infrared Spectroscopy (FTIR)

Fourier transform infrared spectroscopy (FTIR) analysis was performed using a Bruker Censoe 27 FTIR spectrophotometer at room temperature. FTIR spectra were recorded in the range 4,000 to 400 cm^{-1}.

3. Thermogravimetric Analysis (TGA)

Thermogravimetric analysis determines the thermally induced weight change of a sample as a function of temperature. The apparatus used was a Mettler Toledo TGA instrument. The temperature range of analysis was from 25 to 800 °C at a heating rate of 10 °C/min under a nitrogen atmosphere. The mass of the remaining inorganic matter was compared to the dry mass of the starting material.

4. Morphology

Scanning electron microscopy (SEM) was used to examine the membrane surface as well as the cross-section morphology. The samples were prepared by freezing the membranes in liquid nitrogen before breaking them to expose the membrane cross-section. Prior to SEM examination the sample stubs were vacuum sputtered with a thin layer of gold for 4 min to make them electronically conductive. The analysis was performed using a Hitachi 650 SEM.

5. X-ray Diffraction

X-Ray diffraction (XRD) patterns were recorded at room tem-

perature by a Bruker X-ray diffractometer (D_8-Advance) using CuKα (λ=1.54) radiation. Data were obtained in 2θ range of 5-80° with a scanning rate 3/min and with a step size of 2θ equal to 0.05°.

6. Water and Methanol Uptake

The water and methanol uptake was obtained by measuring the weight difference between the fully-hydrated and the dried membrane. A piece of the membrane, with 10 mm×50 mm surface area, was dried in the drying oven at 60 °C for 24 h and weighed (W_{dry}). Then membranes were immersed in de-ionized water and 20 vol% methanol solution at different temperature for 24 h. The membrane was left in de-ionized water and methanol until no further weight gain could be observed. The membranes were then removed from the water and methanol quickly, dry-wiped with soft tissue paper to remove the surface water and methanol, and immediately weighed to determine the membrane's wet mass (W_{wet}). The water and methanol of the uptake membranes was determined using Eq. (1):

$$W_{ut}=\frac{W_{wet}-W_{dry}}{W_{dry}}\times 100\% \quad (1)$$

7. Conductivity Measurements

The membrane conductivity was determined as a function of temperature and relative humidity by impedance spectroscopy with HAMEG - HM8118 analyzer in the frequency range 10 Hz to 1 MHz. Conductivity measurements were carried out on membranes and they were sandwiched between the two stainless steel plates. These electrodes with a contacting area of 0.031 cm^2 were connected to a milliohm meter and horizontally pressed onto the membrane surface to be tested. The membrane resistance was measured as the temperature of the cell from was increased r.t. to 80 °C, while the membrane was kept under water for 24 h.

The conductivity of the samples in the transverse direction was calculated from the impedance data, using the relation s=d/RS, where d and S, designated as thickness and area of the sample, were determined before and after the measurements. The resistance R was derived from the high frequency intercept with the real axis on a complex plane impedance plot. The spectra were analyzed using the Zview® software.

8. Methanol Permeability

Methanol permeability of membranes was determined by a glass diffusion cell composed of two reservoirs, each with a capacity of 100 ml. The membranes were equilibrated in de-ionized water for at least 24 h before any measurement. Each compartment was separated by a pre-hydrated membrane. One reservoir was filled with 20% (v/v) methanol solution (V_A), and the other was filled with de-ionized water (V_B). Each compartment was kept stirring during experiment to ensure the uniformity of the cell concentration. The methanol permeability was found using Eq. (2) [10,38-40]:

$$C_{B(t)}=A/V_B\times P/L\times C_{A(t)}\,(t-t_0) \quad (2)$$

where, C_A and C_B are the concentrations of methanol in the donor and receptor reservoirs, respectively; A and L are the surface area and thickness of the membrane, respectively; P (P=DK) is the methanol permeability ($cm^2\,s^{-1}$); and V_B is the volume of compartment B.

9. Selectivity

An ideal membrane for high performance DMFCs has high proton conductivity and low methanol permeability. To confirm the suitability of the membrane for fuel cell, the selectivity of the membrane was calculated by Eq. (3) [38]:

$$F=S/P \quad (3)$$

where, F is a parameter that evaluates the overall membrane per-

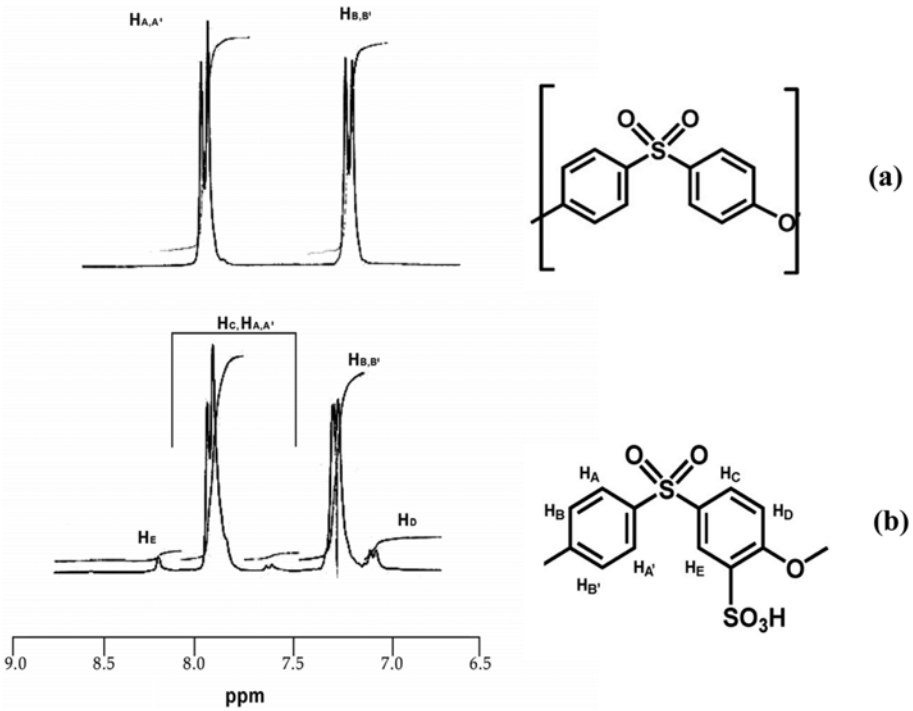

Fig. 2. ^{1}H-NMR of (a) unsulfonated PES and (b) sulfonated PES in d_6-DMSO.

formance in terms of the ratio of proton conductivity (S) to methanol permeability (P).

RESULTS AND DISCUSSION

1. ^{1}H NMR

^{1}H NMR spectroscopy was used for quantitative determination of sulfuric acid groups. The presence of sulfonic acid groups in a repeat unit of polymers was estimated by ^{1}H NMR to determine the location of the peak related to the proton, which would be transferred into lower field. Sulfonated polymers' specific feature was reported through ^{1}H NMR spectroscopy by Nolte et al. for the first time [18]. Figs. 2(a) and 2(b) present the ^{1}H NMR spectra from PES and SPES in DMSO. By comparing these two spectra, we determined that the presence of sulfonic acid groups in polymeric chain results in an apparent transfer of one of the protons in aromatic ring (H_E), to a lower field and higher chemical substitution, in comparison to other protons from the other ring (H_A, H_B, H_C, and H_D). As it could be observed in Fig. 2(b), sulfonic acid group is located in *ortho*-position and the proton (H_E) which is transferred into the lower field is located in *meta*-position of the aromatic ring; also, the number of H_E determines the number of sulfonic acid groups in polymeric matrix [18].

Based on the following equation, the sulfonation degree for PES in an almost 24 h at 55 °C was determined to be 16.94%. In the equation, n is the number of H_E protons in each repeat unit and A_{H_E} and $A_{H_A, B, C, D}$ are related to the integrals under H_E, H_A, H_B, H_C, and H_D peaks and finally, according to Eq. (4) sulfonation degree is calculated from (n×100%) formula [41-44].

$$N(8-2N)=A_{H_E}/\Sigma A_{HA, A', B, B', C, D} \ (0\le n\le 1) \quad (4)$$

2. FTIR

Fig. 3 presents FTIR spectrum of the absorptive peaks from functional groups in SPES, SPES/$SiO_{2(5\%)}$ and SPES/CDI/AS/$SiO_{2(5\%)}$ composite membranes. The presence of -SO_3H groups of SPES is proven by the given IR spectra. The symmetrical stretching absorption of O=S=O is observable at 1,023 cm^{-1} frequency, which is caused by introduction of -SO_3H groups into the SPES chains. Absorption at 873 cm^{-1} is due to aromatic sulfonation groups [45,46]. The broad band at 3,445 cm^{-1} is assigned to O-H hydrogen bonded of SO_3H groups. Fig. 3 shows the IR spectrum of SPES/SiO_2 5% composite membrane. The stretching vibrations at 3,552 cm^{-1} [49] and 1,672-1,587 cm^{-1} [47] are attributed to the hydroxyl groups in Si-OH bond and C=C at the aromatic ring, respectively. The absorption at 3,552 cm^{-1} indicates that the hybrid membrane was made through sol-gel reaction. The stretching vibrations at 3,632-3,500 cm^{-1} are attributed to free O-H of SO_3H groups (acidic group), which have not reacted with SiO_2. The bands at 1,491-1,408 cm^{-1} correspond to the stretching vibration of O=S=O located in *para*-position at the aromatic ring. Two absorption bands at 1,329 and 1,169 cm^{-1} are ascribed to the stretching vibrations of the aromatic ether (C-O-C) [18]. The strong stretching vibrations at 3,096-3,068 cm^{-1} correspond to the aromatic hydrogen (C-H) [48]. The sharp absorption bands at 1,011 and 520 cm^{-1} are assigned to the Si-O and Si-O-Si stretching vibrations, respectively [18,49-51]. By observing the IR spec-

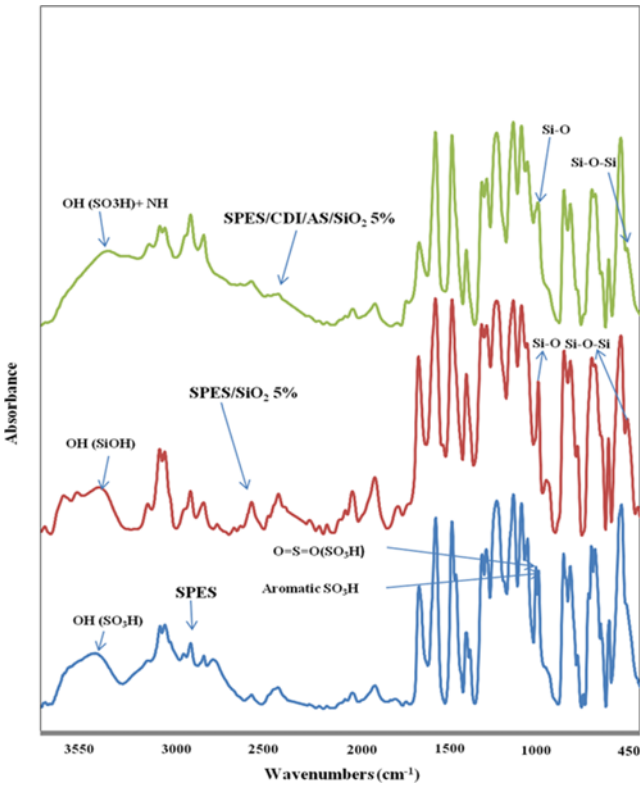

Fig. 3. FTIR spectra of the SPES, SPES/$SiO_{2(5\%)}$ and SPES/CDI/AS/$SiO_{2(5\%)}$ composite membranes.

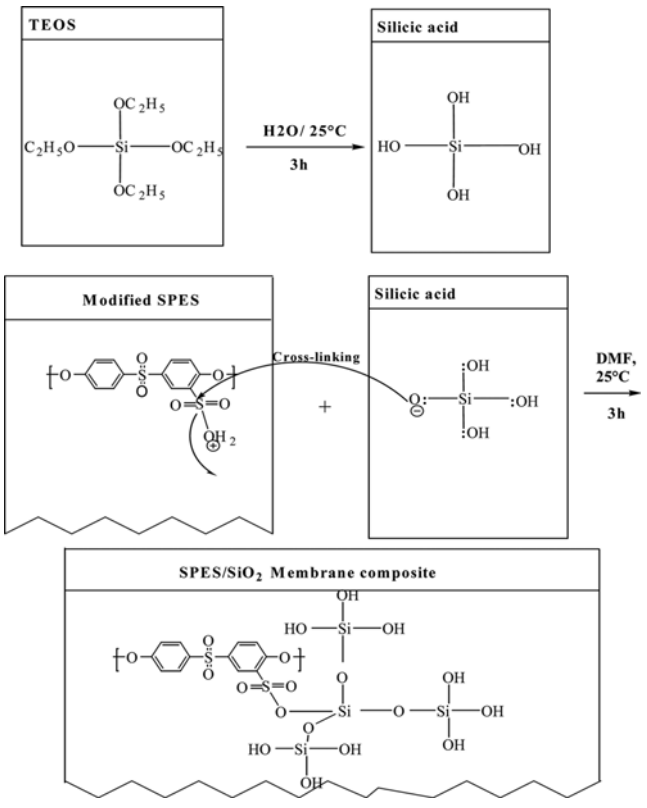

Fig. 4. Scheme of reaction between SPES and SiO_2 and formation of SPES/SiO_2 composite membrane.

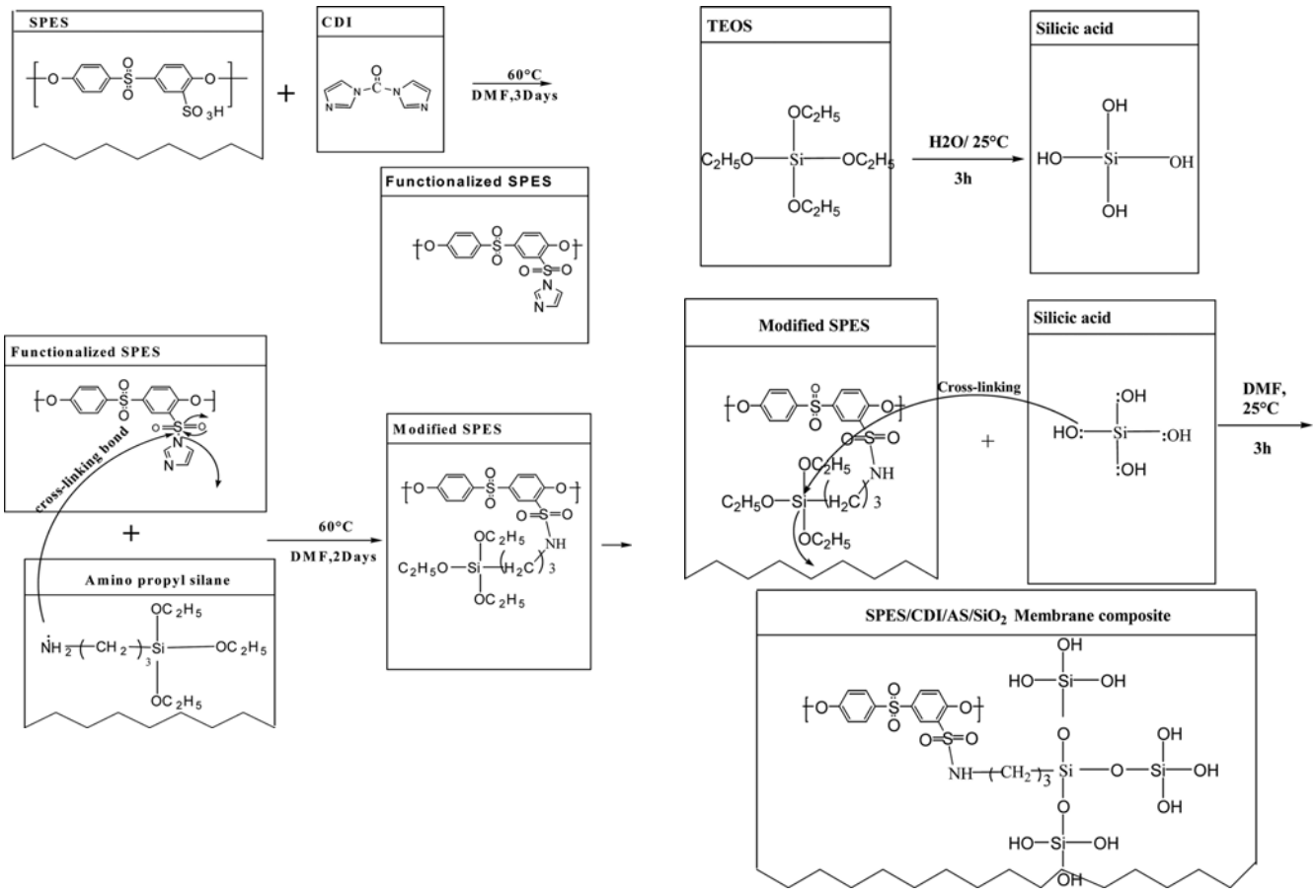

Fig. 5. Scheme of reaction between SPES and CDI, AS and SiO_2 and formation of SPES/CDI/AS/SiO_2 membrane composite.

trum of SPES/CDI/AS/$SiO_{2(5\%)}$ composite membrane, the absorption bands at 3,386 cm^{-1} are attributed to secondary amines stretching vibration (-NH-) and stretching vibration of the hydroxyl group related to Si-OH, which are overlapped in the spectra [48]. The sharp bands at 2,927, 2,855 and 2,592 cm^{-1} are assigned to three -CH_2 stretching vibrations of the grafted groups to secondary amine (-NH-). The peaks at 3,097 cm^{-1}, 1,666-1,583 cm^{-1}, 1,486-1,408 cm^{-1} and 1,327-1,150 cm^{-1} can be attributed to C-H stretching vibrations of the aromatic ring, C=C aromatic ring bands and O=S=O located in *para*-position at the aromatic ring of PES and the stretching vibration of aromatic ether (C-O), respectively [18,47-49]. The obvious absorption bands at 1,014 and 555 cm^{-1} are contributed to the Si-O and Si-O-Si stretching absorptions, respectively [20,49-51]. FTIR results suggest that CDI, AS and SiO_2 have successfully entered the SPES polymeric matrix. The reaction mechanisms between SPES and SiO_2, CDI and AS and formation of SPES/SiO_2 and SPES/CDI/AS/SiO_2 composite membranes are shown in Fig. 4 and Fig. 5, respectively [1,52,53].

3. Thermal Stability

The thermal weight loss of SPES/CDI/AS/$SiO_{2(3,\,5\text{ and }8\%)}$ and SPES/$SiO_{2(5\%)}$ composite membranes was studied by thermogravimetric analysis (Fig. 6). As shown, a two-step degradation of SPES/SiO_2 composite membrane can be observed. The first weight loss appears around 210 °C, which is due to thermal decomposition of sulfonic acid [46,54]. The second degradation step is found above 420 °C due to the thermal degradation of SPES chains [55].

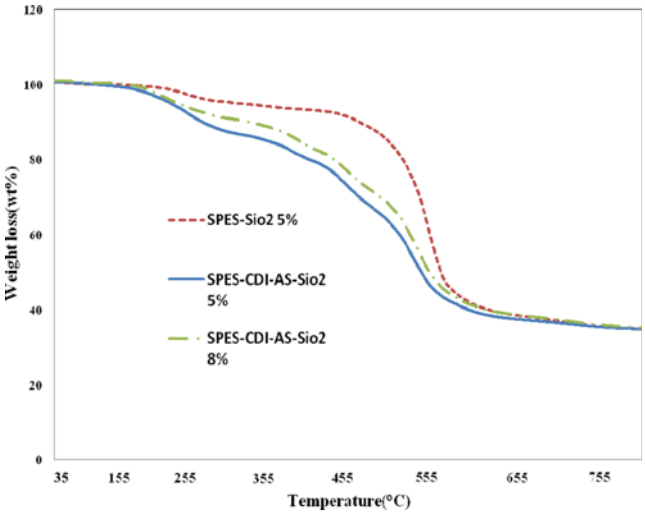

Fig. 6. TGA thermograms of SPES/$SiO_{2(5\%)}$ and SPES/CDI/AS/$SiO_{2(5\text{ and }8\%)}$ versus temperature.

It is evident from Fig. 6 that there are four steps of weight loss on TGA of SPES/CDI/AS/SiO_2 composite membranes. The first and the last degradation temperatures (around 210 °C and 420 °C) were described earlier. The two-step weight loss between 300 °C

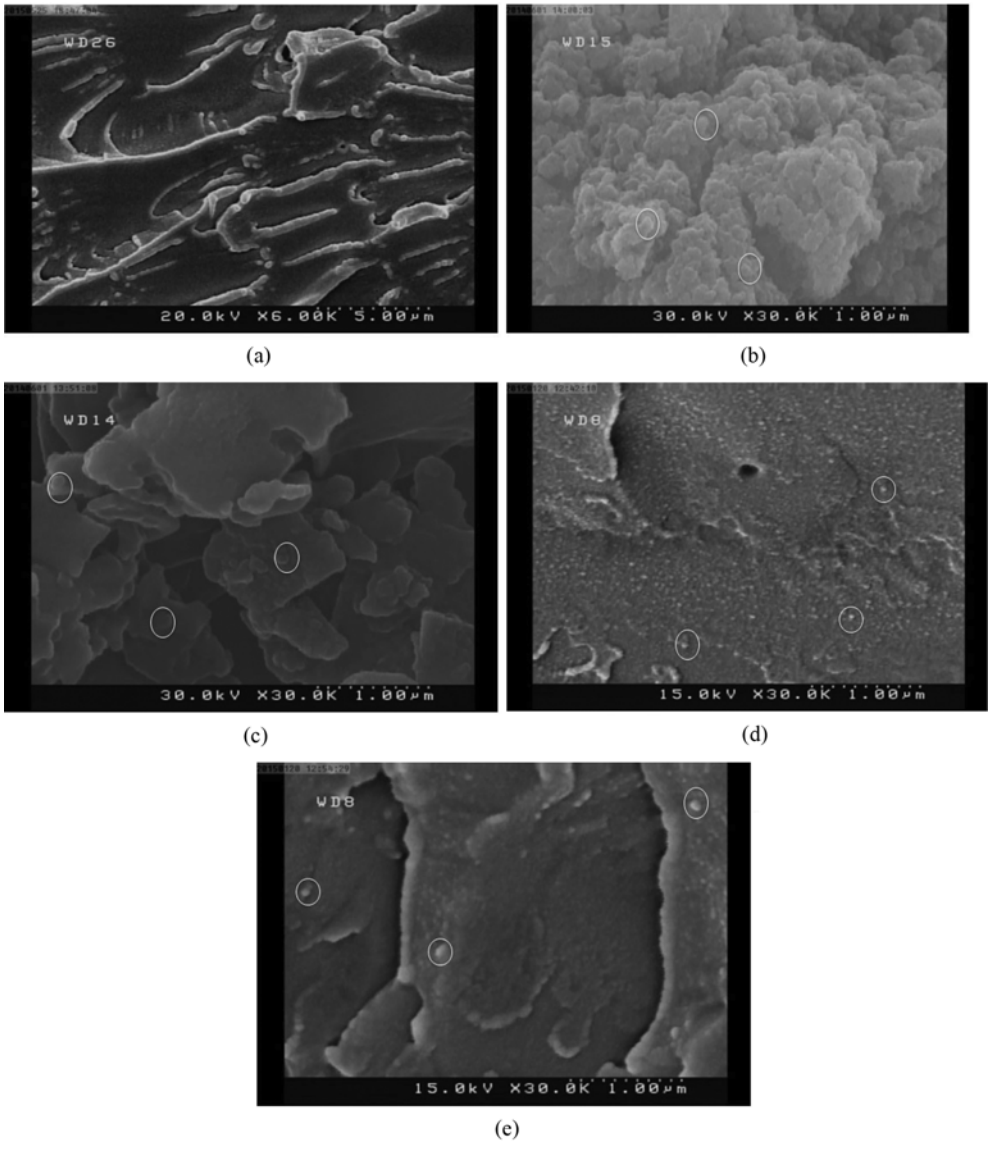

Fig. 7. SEM micrographs of cross-section of (a) pure SPES membrane (b) SPES/CDI/AS/$SiO_{2(5\%)}$, (c) SPES/ $SiO_{2(5\%)}$, (d) SPES/CDI/AS/$SiO_{2(3\%)}$ and (e) SPES/CDI/AS/$SiO_{2(8\%)}$ composite membranes.

and 420 °C may be ascribed to the decomposition of the CDI and AS, which confirms the organic loading of CDI and AS in the composite membranes.

4. SEM

SEM was used to study the morphology of SPES/SiO_2 and SPES/CDI/AS/SiO_2 composite membranes and to observe the nanoparticle distribution in these two systems. Figs. 7(a)-7(e) show the electron micrographs of the cross-sections of SPES, SPES/CDI/AS/SiO_2 and SPES/SiO_2 membranes with various silica content, respectively. As observed in Fig. 7(a), SPES pure membrane has a bulky and homogeneous cross-section. In the images corresponding to composite membranes (Figs. 7(b)-7(e)) which are provided through sol-gel method, a phase-separated morphology is observed inside the membranes. In this morphology, polymer is considered as the matrix phase in which silica nanoparticles are distributed with spherical shape. By comparing SEM images of SPES/CDI/AS/$SiO_{2(5\%)}$ composite membrane with SPES/$SiO_{2(5\%)}$ in Figs. 7(b) and 7(c), it may be seen that SPES/CDI/AS/$SiO_{2(5\%)}$ cross-section shows a more homogeneous and uniform texture with lower cavities, compared to SPES/$SiO_{2(5\%)}$. That is because in SPES/CDI/AS/SiO_2 membrane, the inorganic particles (silica) are distributed within the polymer chains uniformly and homogeneously by the covalent bond with CDI and AS. Hence, nanoparticle agglomeration is lower in such membrane. According to Figs. 7(c)-7(e), we can see that the size of nanoparticles increases along with increases in silica content in the polymeric matrix. In addition, with increase in SiO_2 content, some small aggregates appear in the composites, as shown in Fig. 7(e).

5. XRD

The micrometric structures of the membranes including SPES, SPES/$SiO_{2(5\%)}$ and SPES/CDI/AS/$SiO_{2(5\% \text{ and } 8\%)}$ were studied by XRD. The obtained results are presented in Table 1. XRD pattern from SPES pure membrane (Fig. 8) shows a wide spectrum located at 2θ

Table 1. X-ray diffraction data of the SPES, SPES/$SiO_{2(5\%)}$, SPES/CDI/AS/$SiO_{2(5 \text{ and } 8\%)}$ composite membranes

Samples	Peak position ($2\theta^{o}$)	d-Spacing (A^{o})	FWHM (^{o})
SPES	13.67	6.15	4.03
SPES/$SiO_2$5%	13.55	6.23	4.04
SPES/CDI/AS/$SiO_2$5%	13.28	6.35	5.89
SPES/CDI/AS/$SiO_2$8%	13.25	6.37	4.70

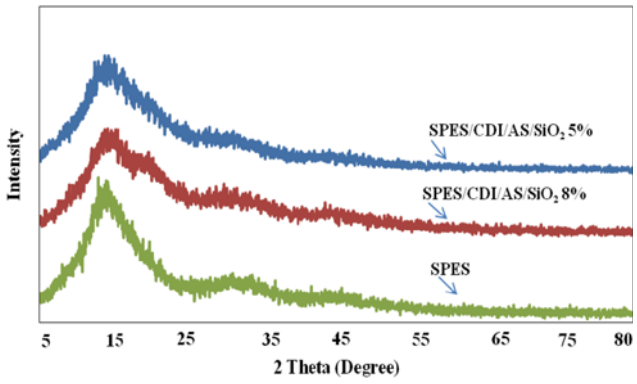

Fig. 8. XRD patterns for SPES, SPES/CDI/AS/$SiO_{2(5 \text{ and } 8\%)}$ composite membranes.

equal to 13.67° and also it determines d-spacing value as 6.15 Å. By adding silica to the SPES polymer matrix, SPES/$SiO_{2(5\%)}$ composite membrane has been prepared. The data of XRD of this compound (Table 1) show that SPES/$SiO_{2(5\%)}$ composite membrane has diffraction angle (2θ) and interplanar spacing values as 13.55° and 6.23 Å, respectively. Also by adding AS, CDI and various content of silica (5% and 8%) to the SPES polymeric matrix, SPES/CDI/AS/$SiO_{2(5\% \text{ and } 8\%)}$ composite membranes were formed. According to XRD results of these compounds in Table 1 and Fig. 8, the main peak of SPES/CDI/AS/$SiO_{2\,(5\% \text{ and } 8\%)}$ composite membranes is located at 2θ equal to13.28° and 13.25°, respectively, and also it determines d-spacing value as 6.35 and 6.37 Å, respectively. By comparing diffraction peaks (2θ) of the modified and unmodified composite membranes, it can be observed that the slight shift in peaks of SPES/CDI/AS/$SiO_{2(5\% \text{ and } 8\%)}$ membranes toward the lower 2θ is due to the addition of CDI and AS in SPES matrix. The relative degree of amorphous phase can be estimated from the full-width at half maximum (FWHM) from the each peak [56]. The FWHM values of SPES/$SiO_{2(5\%)}$ and SPES/CDI/AS/$SiO_{2(5\% \text{ and } 8\%)}$ composite membranes are 4.04°, 5.89° and 4.70°, respectively. Apparently, a bigger FWHM value corresponding to a broadened peak indicates stronger electrostatic cross-linking covalent bonding, which occurs in the SPES/CDI/AS/SiO_2 membrane and increases the amorphous region. This result indicates that macromolecular orientation has decreased within the polymer after incorporation of CDI and AS and formation SPES/CDI/AS/SiO_2 membrane compared with that of SPES/SiO_2 composite membrane.

6. Water and Methanol Uptake

Water uptake in polymeric membranes increases by increases in the degree of sulfonation. The water in the membrane plays the role of a carrier for proton and leads to increase or upkeep of conductivity in polymer. But water uptake leads to excessive inflation of the membrane, which results in reduced resistance of the polymer membrane. Water uptake tests show the water storage, which is one of most influential factors on conductivity. In this study, water uptake and methanol uptake tests were carried out at 25-80 °C, which show a weight difference among dry and wet samples. Fig. 9 and Fig. 10 present the water uptake and methanol uptake diagrams for SPES membrane, compared to SPES/SiO_2 and SPES/CDI/AS/SiO_2 composite membranes; the results are briefly presented in Table 2. It suggests that water uptake and methanol uptake of SPES, SPES/SiO_2 and SPES/CDI/AS/SiO_2 membranes increase with temperature. According to Figs. 9 and 10, water uptake and methanol uptake by the membranes are lowered in the presence of SiO_2. This decrease in water and methanol uptake is mainly due to the decrease in the fraction of sulfonic acid groups per unit membrane weight by forming covalent bonds between -SO_3H in polymeric chain and free OH of silica (Fig. 4) [12]. This leads to the loss of ionic sites to absorb water and methanol molecules, and so water and methanol uptake is decreased. Considering Figs. 9 and 10 and Table 2, it can be observed that water and methanol

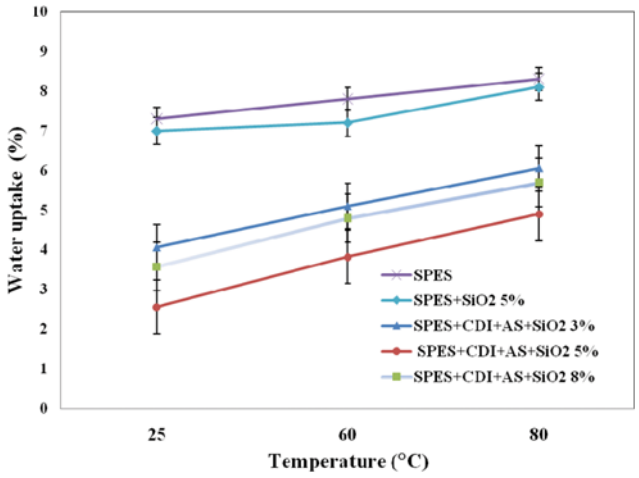

Fig. 9. Water uptake of different membranes versus temperature.

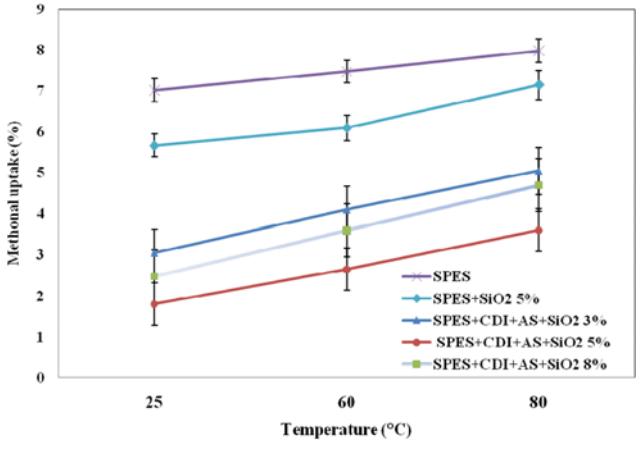

Fig. 10. Methanol uptake of different membranes versus temperature.

Table 2. Water and methanol uptake for the SPES, SPES/$SiO_{2(5)\ \%}$ and SPES/CDI/AS/$SiO_{2(3,\ 5\ and\ 8)\ \%}$ composite membranes

	Water uptake (%)			Methanol uptake (%)		
Samples	25 °C	60 °C	80 °C	25 °C	60 °C	80 °C
SPES	7.30	7.80	8.30	7.02	7.48	7.99
SPES/$SiO_2$5%	6.99	7.20	8.10	5.67	6.10	7.15
SPES/CDI/AS/$SiO_2$3%	4.06	5.10	6.05	3.05	4.1	5.05
SPES/CDI/AS/$SiO_2$5%	2.56	3.82	4.90	1.80	2.65	3.60
SPES/CDI/AS/$SiO_2$8%	3.58	4.80	5.70	2.48	3.59	4.70

uptake in SPES/CDI/AS/SiO_2 composite membrane shows a considerable drop. Treatment of polymer matrix with CDI and AS before the use of TEOS seems to ensure a uniform dispersion and adhesion between the organic and inorganic phases. Therefore, the adhesion between the phases was improved by such modification, which led to reduced free volume. By comparing water uptake and methanol uptake results, related to SPES/CDI/AS/SiO_2 composite membrane with various silica percentages, it can be observed that by increase in silica percentage from 3% to 5 wt% water and methanol uptake drastically decreases in the membrane. This result is due to the cross-linking of polymeric chains by formation of covalent bonds between CDI, AS and nanosilica. On the other hand, by the increase in silica content to 8 wt%, water and methanol uptake displays a slight increase compared to 5 wt%, which is due to the agglomeration of nanoparticles within the matrix. Also, the water and methanol uptake values of the SPES membrane, composite membranes and Nafion 117 were compared at 25 °C and the results are listed in Table 4. Compared with Nafion 117 membrane, all the SPES/CDI/AS/SiO_2 and SPES/SiO_2 composite membranes showed lower water and methanol uptake.

7. Proton Conductivity

Proton conductivity is a significant feature of fuel cell membranes that has an impact on their application and other influence. Table 3 presents the proton conductivity results at 25-80 °C. As observed in Table 3, the conductivities of all membranes increase by increases in temperature. This could be due to the movement of water molecules and structural re-orientation, which is as important as increased molecular mobility [20]. Considering Table 3, proton conductivity in composite membranes in many cases is lower than SPES pure membrane in temperature range between 25 °C and 80 °C, because silica nanoparticles form covalent structure with sulfonic acid groups (-SO_3H) in polymeric chains leading to loss of ionic sites and lowered conductivity [20]. Table 3 shows that in SPES/CDI/AS/SiO_2 composite membranes, proton conductivity increases by decreasing cavities in the composites when compared to SPES/SiO_2 samples. This is because adding CDI and AS and forming cross-linking covalent bond between silica and polymeric chain can lead to increased adhesion between the organic and inorganic phases that results in good dispersion of silica particles and prevention of the agglomeration to some extent. According to SEM results, the cavities in membrane polymeric structure decrease by the increase of silica content from 3% to 5% and increase from 5% to 8% due to partial agglomeration of SiO_2. Therefore, the best composite membrane that shows lower water and methanol uptake is found to be SPES/CDI/AS/$SiO_{2(5\%)}$ and presents lower proton conductivity when compared to SPES/CDI/AS/$SiO_{2(3\%\ and\ 8\%)}$. Greater compaction in SPES/CDI/AS/$SiO_{2(5\%)}$ membrane leads to obstruction of polymer chain movement in the ionic cluster. By comparing SPES/CDI/AS/$SiO_{2(5\%)}$ and SPES/$SiO_{2(5\%)}$ composite membranes, according to Table 3, proton conductivity in SPES/CDI/AS/$SiO_{2(5\%)}$ membrane is higher that of SPES/$SiO_{2(5\%)}$ membrane. This is attributed to the presence of two CDI and AS compounds, that by forming covalent bonds with polymeric chain there would be better and more uniform distribution of SiO_2 in polymeric membrane and could lead to lower cavities which function as dielectrics. This has led to an increase in proton conductivity in SPES/CDI/AS/$SiO_{2(3\%,\ 5\%\ and\ 8\%)}$ membranes compared to SPES/$SiO_{2(5\%)}$. According to the suggested mechanism (Fig. 11), in order to have a continuous pathway for the H_3O^+, no gap should be presented so that proton can move through hydrogen bonding along the polymer chain direction. Also, the proton conductivity values of the pure SPES membrane, SPES/CDI/AS/SiO_2, SPES/SiO_2 composite membranes and commercial Nafion are compared and the results are listed in Table 4.

The proton conductivity of the Nafion 117 was 0.017 s cm^{-1} at room temperature. In comparison with Nafion 117, the proton conductivity of SPES membrane (0.0135 s cm^{-1}) and SPES/CDI/AS/$SiO_{2(3\%,\ 5\%\ and\ 8\%)}$ composite membranes that were 0.0180, 0.0134

Table 3. Proton conductivity for the SPES, SPES/$SiO_{2(5\%)}$ and SPES/CDI/AS/$SiO_{2(3,\ 5\ and\ 8\%)}$ composite membranes

	Conductivity (s/cm)			
Samples	25 °C	40 °C	60 °C	80 °C
SPES	0.0135±0.002	0.0245±0.002	0.0362±0.002	0.0402±0.002
SPES/$SiO_2$5%	0.0056±0.002	0.0102±0.002	0.0155±0.002	0.0174±0.002
SPES/CDI/AS/$SiO_2$3%	0.0180±0.002	0.0192±0.002	0.0234±0.002	0.0275±0.002
SPES/CDI/AS/$SiO_2$5%	0.0134±0.002	0.0152±0.002	0.0163±0.002	0.0174±0.002
SPES/CDI/AS/$SiO_2$8%	0.0186±0.002	0.0213±0.002	0.0253±0.002	0.0282±0.002

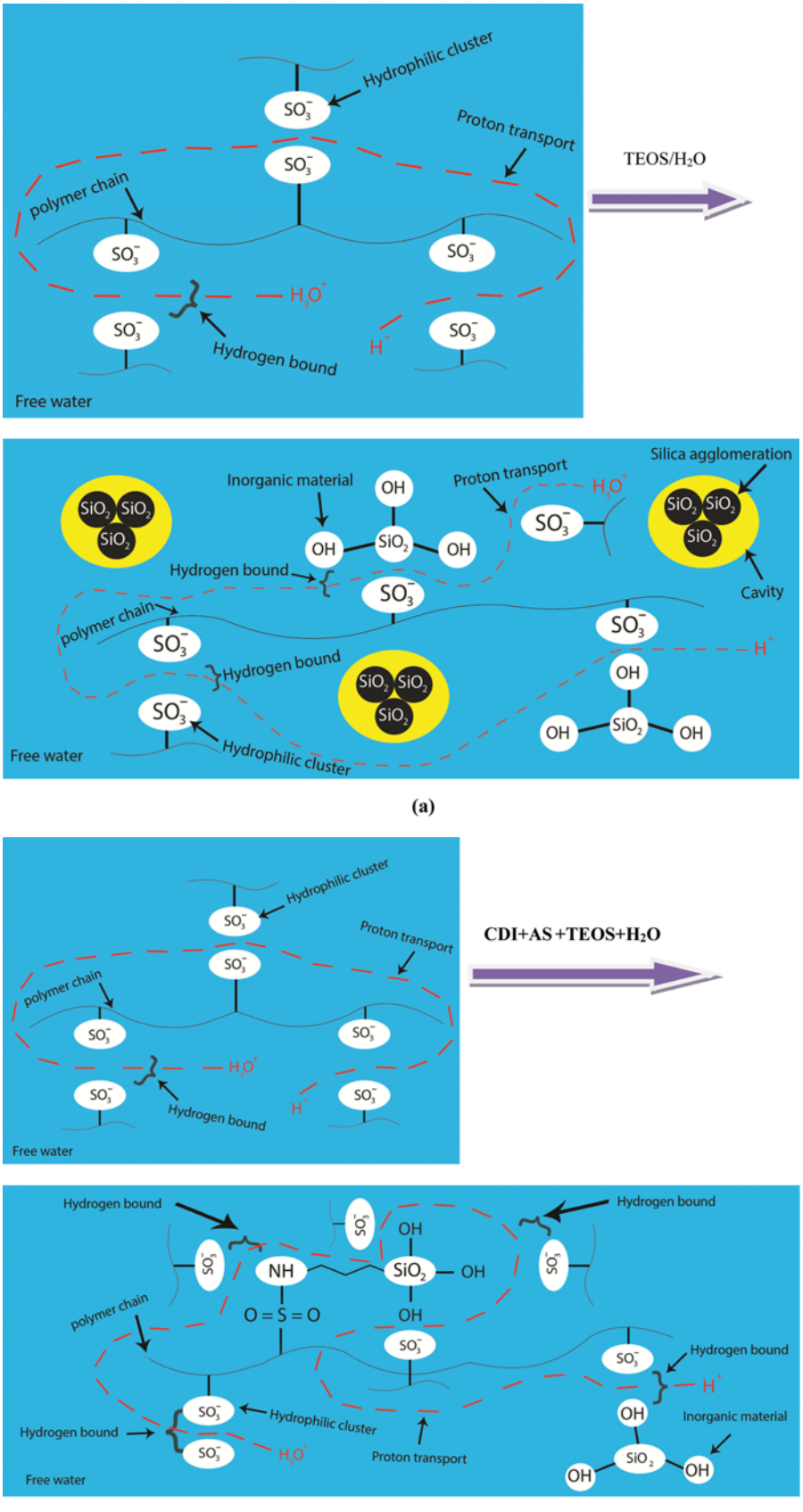

Fig. 11. Representative view of proton transport in (a) SPES/SiO_2 and (b) SPES/CDI/AS/SiO_2 composite membranes including CDI, AS and SiO_2 particles.

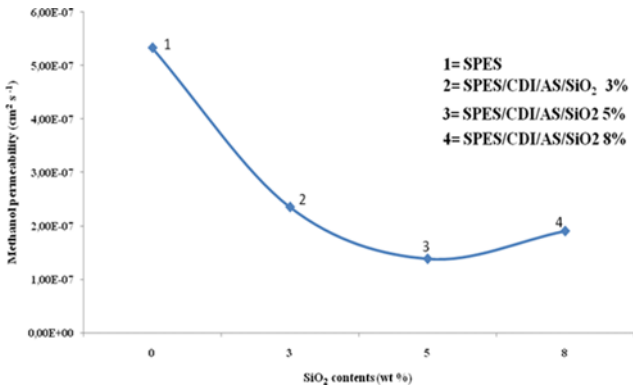

Fig. 12. Methanol permeability of SPES and SPES/CDI/AS/$SiO_{2(3, 5 and 8\%)}$ composite membranes.

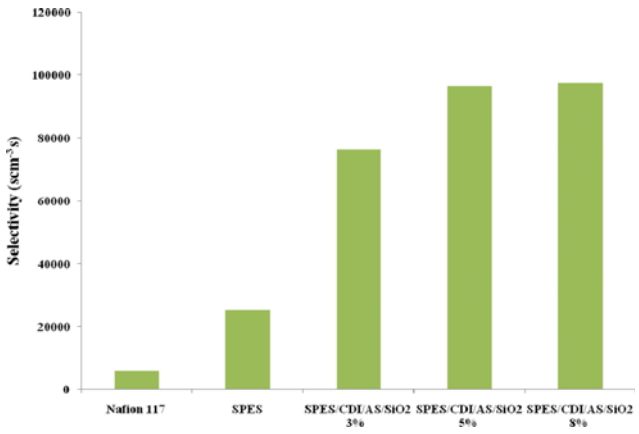

Fig. 13. Selectivity of Nafion 117[57], SPES and SPES/CDI/AS/$SiO_{2(3, 5 and 8\%)}$ composite membranes.

and 0.0186 s cm^{-1}, in the stated order, have approached the proton conductivity of Nafion 117.

8. Methanol Permeability

Fig. 12 shows the methanol permeability as a function of SiO_2 content for pure SPES membrane and SPES/CDI/AS/$SiO_{2(3, 5 and 8\%)}$ composite membranes. The methanol permeability values of the composite membranes and Nafion 117 membrane at room temperature for better comparison are listed in Table 4. Methanol permeability for the SPES membrane is found to be 5.34×10^{-7} cm^2 s^{-1}, which reduces to 2.36×10^{-7} cm^2 s^{-1} for SPES/CDI/AS/$SiO_{2(3\%)}$ and 1.39×10^{-7} cm^2 s^{-1} for SPES/CDI/AS/$SiO_{2(5\%)}$ membranes and finally reaches 1.91×10^{-7} cm^2 s^{-1} for SPES/CDI/AS/$SiO_{2(8\%)}$ membrane. The results show that the incorporation of SiO_2 lowers methanol permeability because the nano-sized dispersion of silica prevents methanol from migrating through the membrane and the covalent cross linking structure between modified sulfonic acid (-SO_3H) groups of SPES and SiO_2 (Fig. 5) restricts the formation of channels in the membranes, which reduces methanol permeability [2,9]. With increasing silica loading from 0 to 5 wt%, the methanol permeability is decreased. However, a further increase in silica loading to 8 wt% did not contribute to any additional drop in methanol permeability. At low silica loading, the hydrophilic silica particles mainly exist around the hydrophilic ionic clusters and the ionic channels, which leads to changes in the microstructure of SPES and increases the tortuosity of the methanol transport channels. At higher silica loading, hydrophilic silica may exist among the structure of the polymer chains that increases the contribution of the hydrophobic polymer backbones for methanol permeation [56]. Note that compared with Nafion 117 membrane (Table 4), all the SPES/CDI/AS/SiO_2 composite membranes display lower methanol permeability.

9. Selectivity

Fig. 13 and Table 4 show the selectivity of the SPES, Nafion 117 and SPES/CDI/AS/SiO_2 composite membranes with various content of silica at room temperature. The selectivity of a membrane is considered as proportional to the membrane conductivity and inversely proportional to the methanol permeability. A higher selectivity value implies better applicability in DMFCs. The selectivity of the SPES membrane was significantly improved with the introduction of CDI, AS and silica; and SPES/CDI/AS/SiO_2 membranes showed better performance compared to Nafion 117 (Table 4). The maximum selectivity appears at 8 wt% silica loading. Therefore, SPES/CDI/AS/SiO_2 composite membranes are definitely promising materials for DMFCs.

CONCLUSION

SPES/CDI/AS/SiO_2 composite membranes with various silica loadings were prepared and compared with SPES/SiO_2 membrane. Adding CDI and AS to the polymeric matrix and its modification

Table 4. Water uptake, methanol uptake, proton conductivity, methanol permeability and selectivity of Nafion 117, SPES and SPES/CDI/AS/$SiO_{2(3, 5 and 8\%)}$ composite membranes at room temperature

Sample	Water uptake (%)	Methanol uptake (%)	Proton conductivity (s cm^{-1})	Methanol permeability $\times10^{-7}$ cm^2 s^{-1}	Selectivity $\times10^3$ $scm^{-3}s$
SPES	7.30	7.02	0.013	5.34	25.280
SPES/CDI/AS/$SiO_{2(3\%)}$	4.06	3.05	0.018	2.36	76.271
SPES/CDI/AS/$SiO_{2(5\%)}$	2.56	1.80	0.013	1.39	96.402
SPES/CDI/AS/$SiO_{2(8\%)}$	3.58	2.48	0.019	1.91	97.382
Nafion 117 [57]	-	-	0.014	28.3	5.053
Nafion 117 [10]	33	-	0.017	29.1	6.013
Nafion 117 [2]		-	0.015	10.0	15.000
Nafion 117 [40]	17	30	0.032	12.4	25.806

prior to in situ generation of silica and then formation of covalent cross-linking structure led to a more uniform distribution of SiO_2 in the polymeric matrix. The effect of CDI, AS and silica addition in composite membranes was studied by thermal stability, water and methanol uptake, morphology, proton conductivity, methanol permeability and selectivity. Modification of SPES matrix with CDI and AS before in situ generation of SiO_2 decreased methanol permeability, water and methanol uptake in SPES/CDI/AS/SiO_2 membranes in comparison with SPES and SPES/SiO_2 membranes. Water uptake, methanol uptake and methanol permeability tests indicated that 8 wt% silica in the SPES/CDI/AS/SiO_2 composite membrane can significantly decrease the swelling of the composites, and also can decrease crossover of methanol molecules without a large drop in proton conductivity, e.g., 13.06% at 40 °C. Hence, among the prepared composite membranes, SPES/CDI/AS/$SiO_{2(8\%)}$ can be considered the best composite membrane for application in DMFCs as the electrolyte, as it features a good balance between high proton conductivity and low methanol and water uptake.

REFERENCES

1. S. P. Nunes, B. Ruffmann, E. Rikowski, S. Vetter and K. Richau, *J. Membr. Sci.*, **203**, 215 (2002).
2. Z. Gaowen, J. Jiuxin and L. J. ianing, *J. Wuhan University of Technology-Mater. Sci. Ed.*, **26**, 417 (2011).
3. D. Prasanna and V. Selvaraj, *Korean J. Chem. Eng.*, **33**(4), 1489 (2016).
4. N. Chaisubanan, K. Pruksathorn, H. Vergnes and M. Hunsom, *Korean J. Chem. Eng.*, **32**(7), 1305 (2015).
5. T. Yang, S. X. Zhang, Y. Gao, F. C. Ji and T. W. Liu, *J. Fuel*, **1**, 4 (2008).
6. F. R. Kalhammer, P. R. Prokopius, V. P. Roan and G. E. Voecks, State of California Air Resources Board, California (1998).
7. M. Rikukawa and K. Sanui, *J. Prog. Polym. Sci.*, **25**, 1463 (2000).
8. S. Gahlot, V. Kulshrestha, G. Agarwal and P. K. Jha, *J. Macromol. Symp.*, **357**, 173 (2015).
9. S. Gahlot, P. P. Sharma, H. Gapta, V. Kulshrestha and P. K. Jha, *RSC Adv.*, **4**, 24662 (2014).
10. Y. Heo, H. Im and J. Kim, *J. Member. Sci.*, **425**, 11 (2013).
11. Y. Woo, S. Y. Oh, Y. S. Kang and B. Jung, *J. Membr. Sci.*, **220**, 31 (2003).
12. S. M. Park, Y. W. Choi, T. H. Yang, J. S. Park and S. H. Kim, *Korean J. Chem. Eng.*, **30**, 87 (2013).
13. L. Jorissen, V. Gegel, J. Kerres and J. Garche, *J. Power Sources*, **105**, 267 (2002).
14. S. D. Mikhailenko, S. M. J. Zaidi and S. Kaliaguine, *J. Polym. Sci., Polym. Phys. Ed.*, **38**, 1386 (2000).
15. I. Honma, Y. Takeda and J. M. Bae, *Solid-State Ion*, **120**, 255 (1999).
16. G. Alberti, M. Casciola, L. Massinelli and B. Bauer, *J. Membr. Sci.*, **185**, 73 (2001).
17. B. S. Pivovar, Y. Wang and E. L. Cussler, *J. Membr. Sci.*, **154**, 155 (1999).
18. M. L. Di Vona, E. Sgreccia, M. Tamilvanan, M. Khadhraoui, C. Chassigneux and P. Knauth, *J. Membr. Sci.*, **354**, 134 (2010).
19. S. Swier, V. Ramani, J. M. Fenton, H. R. Kunz, M. T. Shawa and R. A. Weiss, *J. Membr. Sci.*, **256**, 122 (2005).
20. S. Weng, C. Gong, W. C. Tsen, Y. C. Shu, F. C. Tsai and J. T. Yeh, *J. Appl. Polym. Sci.*, **123**, 646 (2012).
21. J. M. Haack, C. Vogel, W. Butwilowski and D. Lehmann, *J. Appl. Chem.*, **79**, 2083 (2007).
22. W. Mabrouk, L. Ogier, S. Vidal, C. Sollogoub, F. Matoussi and J. F. Fauvarque, *J. Membr. Sci.*, **452**, 263 (2013).
23. Bi. P. Tripathi and V. K. Shahi, *J. Polym. Sci.*, **36**, 945 (2011).
24. S. Gahlot, P. P. Sharma, H. Gupta, P. K. Jha and V. kulshrestha, *Adv. Electrochemistry*, **2**, 90 (2014).
25. R. P. Pandey, A. K. Thakur and V. K. Shahi, *ASC Appl. Mater. Interfaces*, **6**, 16993 (2014).
26. S. Gahlot, P. P. Sharma and V. Kulshrestha, *Sep. Sci. Technol.*, **50**, 446 (2014).
27. N. N. Fathima, D. Lawrence, U. Yugandhar, T. S. R. Moorthy and B. U. Nair, A review, *J. Sci., Ind. Res.*, **66**, 209 (2007).
28. T. S. Guth, J. Baurmeister, G. Frank and R. Knauf, *International Patent WO*, **99**, 29763 (1999).
29. S. R. S. Kumar, N. Kurra and H. N. Alshareef, *J. Mater. Chem. C.*, **4**, 215 (2016).
30. F. G. Wilhelm, I. G. M. Punt, N. F. A. van der Vegt, H. Strathmann and M. Wessling, *J. Membr. Sci.*, **199**, 167 (2002).
31. K. D. Kreuer, *J. Membr. Sci.*, **185**, 29 (2001).
32. Y. D. Premchand, M. L. D. Vona and P. Knauth, Ionic Conducting Materials and Structural Spectroscopes, Springer (2008).
33. B. Liu, D. S. Kim, M. D. Guiver, Y. S. Kim and B. S. Pivovar, Membranes for Energy Conversion, Wiley (2008).
34. P. X. Xing, G. P. Robertson, M. D. Guiver, S. D. Mikhailenko, K. P. Wang and S. Kaliaguine, *J. Membr. Sci.*, **229**, 95 (2004).
35. S. Gahlot, P. P. Sharma, B. M. Bhil, H. Gupta and V. Kulshrestha, *J. Macromol. Symp.*, **357**, 189 (2015).
36. S. Gahlot, P. P. Sharma, V. Kulshrestha and P. K. Jha, *J. ACS Appl. Mater. Interfaces*, **6**, 5595 (2014).
37. Y. He, H. Zhang, Y. Li, J. Wang, L. Ma, W. Zhang and J. Liu, *J. Mater. Chem. A*, **3**, 21832 (2015).
38. K. Ahn, M. Kim, K. Kim, I. Oh, H. Ju and J. Kim, *J. Polym.*, **56**, 178 (2015).
39. Y. S. Park and Y. Yamazaki, *Solid State Ionics*, **176**, 1079 (2005).
40. K. Dutta, S. Das and P. P. Kundu, *J. Membr. Sci.*, **468**, 42 (2014).
41. R. Y. M. Huang, P. Shao and C. M. Burns, *J. Appl. Polym. Sci.*, **82**, 2651 (2001).
42. S. Xue and G. Yin, *J. Eur. Polym.*, **42**, 776 (2006).
43. H. L. Wu, C. C. M. Ma and F. Y. Liu, *J. Eur. Polym.*, **42**, 1688 (2006).
44. G. P. Robertson, S. D. Mikhailenko and K. Wang, *J. Membr. Sci.*, **219**, 113 (2003).
45. G. Zundel, *J. Membr. Sci.*, **11**, 249 (1982).
46. M. L. Di Vona, D. Marani, C. D'Ottavi, M. Trombetta, E. Traversa, I. Beurroies, P. Knauth and S. Licoccia, *J. Chem. Mater.*, **18**, 69 (2006).
47. S. Fujiyama, J. Ishikawa, T. Omi and S. Tamai, *J. Polym.*, **40**, 17 (2008).
48. A. Ebadi Amooghin, A. Kargari and M. R. Omidkhah, *J. Membr. Sci.*, **490**, 364 (2015).
49. D. S. Kim, K. H. Shin, H. B. Park and Y. M. Lee, *J. Macromol. Res.*, **12**, 413 (2004).
50. F. Dolatzadeh, S. Moradian and M. M. Jalili, *Corros. Sci.*, **53**, 4248 (2011).
51. Sh. Hassanajili, M. A. Khademi and P. Keshavarz, *J. Membr. Sci.*,

453, 369 (2014).
52. A. K. Sahu, G. Selvarani, S. Pitchumani, P. Sridhar and A. K. Shukla, *J. Electrochem. Soc.*, **154**, B123 (2007).
53. J. Livage, *Curr. Opin. Solid State Mater. Sci.*, **2**, 132 (1997).
54. B. Maranesi, H. Hou, R. Polini, E. Sgreccia, G. Alberti, R. Narducci, P. Knauth and M. L. D. Vona, *Fuel*, **2**, 107 (2013).
55. S. Xue and G. Yin, *J. Electro. Acta*, **52**, 847 (2006).
56. S. Wen, C. Gong, W. C. Tsen, Y. C. Shu and F. C. Tsai, *J. Appl. Polym. Sci.*, **116**, 149 (2010).
57. C. H. Wang, C. C. Chen, H. C. Hsu, H. Y. Du, C. P. Chen, J. Y. Hwang, L. C. Chen, H. C. Shih, J. Stejskal and K. H. Chen, *J. Power Sources*, **190**, 279 (2009).